Asian Journal of Research and Reviews in Physics

4(3): 22-28, 2021; Article no.AJR2P.69367
ISSN: 2582-5992

Far-field to Near-field Data Relations for the Inverse Electromagnetic Scattering Problem

Arnold Abramov[1] and Yutao Yue[1*]

[1]Institute of Deep Perception Technology, Wuxi, China.

Authors' contributions

This work was done in collaboration between both authors. Author AA designed the study. Author YY performed the analysis, wrote the draft of the manuscript and supervised the study. Author AA developed matlab code for calculations. Both the authors managed the literature search writing of the final manuscript, read and approved the final manuscript.

Article Information

DOI: 10.9734/AJR2P/2021/v4i330144
Editor(s):
(1) Dr. Jelena Purenovic, Kragujevac University, Serbia.
Reviewers:
(1) Vladimir Pinchuk, Baltic State Technical University Russia.
(2) Suresh P, Veltech, India.
Complete Peer review History: http://www.sdiarticle4.com/review-history/69367

Original Research Article

Received 01 April 2021
Accepted 09 June 2021
Published 15 June 2021

ABSTRACT

This paper considers (in general form) the problem of recovering information (size and material parameters) about the scattering object from far-field measurements. The order of solution and functions of each equation for the fields inside and outside the scattering object are discussed. Using well-known mathematical theorems, a simple equation has been derived that connects the far-field data on one side to the near-field data on the other side. Consequently, this equation has been used in an optimization procedure to find the parameters of the dielectric cylinder.

Keywords: Electromagnetic wave; scattering; inverse; cylinder; field.

1. INTRODUCTION

If a set of functions and parameters defining the model is given, then the task of obtaining information about the state or properties of the model falls into the category of forward problems. In the opposite case, if some functions or parameters of the model are to be restored, then we are dealing with the inverse problem. The absence of an initial set of data, as well as

**Corresponding author: E-mail: yueyutao@idpt.org;*

complete information about the model, can lead to a number of difficulties when solving inverse problems: the data may not be sufficient to ensure the uniqueness of the solution; quite often, the unknown function or parameter is included in the functional equation in a nonlinear way; the initial information is approximately known due to some errors in the measuring device; the solution of the inverse problem does not continuously depend on the initial data. In addition, it should be noted that the degree of complexity and the methods for solving forward and inverse problems are not equivalent, and that each problem requires special considerations. The rigorous mathematical foundations of the inverse problem theory were developed in the second half of the last century (the main results can be found in the monograph [1]), while there has been an interest regarding the inverse time-harmonic electromagnetic wave scattering problem, which has been intensively developed in the last three decades. The reasons for this time gap are due to the complexity of the combined system of electric and magnetic field equations, which necessitates the imposition of additional assumptions about the incident illumination and the nature of the scatterer, and the difficulties originating from the much more complicated regularity of the solutions of Maxwell's equations are more theoretically robust than those of elliptic partial differential equations. Nevertheless, the development of computational techniques, as well as the relevance and importance of the electromagnetic wave backscattering problem, have stimulated significant progress in this problem over the past two decades. It is worth noting that the approach of using inverse wave scattering studies is non-intrusive to the object under study. To implement it, we only need to collect the scattered fields outside the object non-destructively. Therefore, it has a wide range of applications in various fields, such as radar and sonar imaging [2,3], geophysics [4], medical imaging [5], remote sensing [6], biomedical imaging and diagnostics [7].

Iterative methods are usually widely used to solve the inverse scattering problem (ISP). An iterative procedure employing equivalent Neumann series solutions in each iteration step was proposed in [8] to solve the two-dimensional inverse scattering problem. An iterative algorithm for reconstructing the three-dimensional complex-valued refractive index of an object was proposed in [9]. As a result of the conjugate gradient method in Ref. [10], the ISP was reformulated as an optimization problem, which was solved iteratively. Another popular method is the linear sampling method (LSM), which consists of solving the far-field integral equation for an unknown angular function of the far-field pattern [11,12]. The domain derivatives employed in [13] were used to solve the inverse electromagnetic scattering problem for perfect conductivity or penetrable obstacles. A variational approach targeting the interior transmission problem emerged from the proposed ISP study [14]. The reconstruction of the refractive index from experimental backscattering data using a globally convergent inverse method has been realized in [15]. Furthermore, it is worth noting that the so-called photonic nanojet discovered in this century [16] is an example of the successful revisiting of even well-known effects using modern computing techniques. In [17,18], it became clear that the solution of ISPs for objects capable of generating nanojets leads to new implemented practical applications.

Although numerical methods seem to be more reliable and offer greater possibilities, semi-analytical methods can provide a qualitative analysis of the final results and, in addition, control the accuracy of the results. The method used by us is a symbiosis of both approaches. By transforming the original equation into the difference between the modeled and measured scattered fields, we can determine any parameter based on the minimization conditions. As an illustration of the possibility of the developed optimization process, we found the parameters of the scatterer – radius and dielectric constant of the cylinder. The advantages of the presented approach are convenient and physically meaningful functional relations between near-field and far-field data, as well as controlled accuracy of the results.

2. THE SOLUTION OF MAXWELL'S EQUATIONS FOR THE SCATTERED FIELD

For TM polarized electromagnetic fields (nonzero electric E_z and magnetic H_x, H_y field components), Maxwell's equations are transformed into Helmholtz equations for the electric field as

$$\nabla^2 E_z(x,y) + k^2 \varepsilon E_z(x,y) = 0 \qquad (1)$$

where $k=2\pi/\lambda$, λ is the wavelength and ε is the dielectric permittivity. The cylinder is assumed to have the same permeability as free space. Introducing free space (ε=1) Green function $G(\vec{r},\vec{r}') = \frac{1}{4i} H_0^{(2)}(k \mid \vec{r} - \vec{r}'|)$, we obtain:

$$E_z(\vec{r}) = E_z^{inc}(\vec{r}) - \frac{ik^2}{4}\int (\varepsilon_c - 1) E_z(\vec{r}') H_0^{(2)}(k \mid \vec{r} - \vec{r}'|) d\vec{r} \quad (2)$$

Here $\vec{r} = (x, y)$, $H_0^{(2)}$ is the zero-order Hankel function, ε_c is the dielectric permittivity of the cylinder. The next step is use the method developed in [19]. We divide the cross section of the dielectric cylinder into *N* cells so that the dielectric constant and the electric field intensity of each cell can be assumed to be constant. The integral equation (1) for the electric field is then transformed to the next equation:

$$E_m = E_m^{inc} - \frac{ik^2}{4}\sum_{n=1}^{N} (\varepsilon_n - 1) E_n \int_{cell\ n} H_0^{(2)}(k\rho) dx' dy' \quad (3)$$

where E_n and ε_n denote electric field intensity and the dielectric constant at the centre of cell *n*, respectively, and $\rho = \sqrt{(x'-x_m)^2 + (y'-y_m)^2}$. Replacing a cell with a circle having the same square, we obtain an exact solution for the integral over the Hankel function:

$$\frac{ik^2}{4}\int_0^{2\pi}\int_0^{a} H_0^{(2)}(k\rho)\rho d\rho d\varphi = \begin{cases} i/2\left(\pi ka H_1^{(2)}(ka) - 2i\right), & m = n \\ i\pi ka/2 J_1(ka) H_0^{(2)}(k\rho_{mn}), & m \neq n \end{cases} \quad (4)$$

where ρ and φ are the polar coordinates based on a coordinate origin at the centre of cell *n*, *a* is the radius of a circular cell, J_1 denotes the Bessel function of the first order.

Let us introduce notations for the left-hand side of (3) and (4): E_L, $H_{L,c}$ and E_c, $H_{c,c}$ for $\vec{r}$ being outside and inside the cylindrical cross section *C* respectively. Thus from (3) we have 2 equations:

$$E_L = E_L^i - H_{L,c} X, \quad \vec{r} \notin C \quad (5)$$

$$E_c = E_c^i - H_{c,c} X, \quad \vec{r} \in C \quad (6)$$

where E_L^i and E_c^i are expressed as the incident fields determined at the points lying along line placed at some fixed distance *L* from the cylinder and inside the cylinder respectively, and so-called contrast function:

$$X=(\varepsilon_n-1)E_c=p\,E_c$$

has been introduced. It is worth mentioning that all quantities in (5-6) denoted by *E* are vectors, while the rest are matrices.

Solving (6) for E_c and then using it in (5) we obtain

$$E_L = E_L^i - H_{L,c}[1/(\varepsilon_n - 1) + H_{c,c}]^{-1} E_c^i \quad (7)$$

Eq. (7) actually represents the solution to the forward problem: for a given material parameter and sample size, we can calculate the scattered field. However, the solution to the inverse problem cannot be obtained automatically from (7). That is, if we assume that the scattered field is given, we can calculate *X* from (5) and then calculate E_c from (6), and the ratio $X/E_c = p$ will yield the values of dielectric permittivity. The difficulty arises here in the first step. The matrix $H_{L,c}$ is ill-conditioned; therefore, it is not possible to calculate its inverse one, which is necessary for solving the inverse problem. We also note the nonlinear character of the equations with respect to the unknown contrast function *X*. The non-symmetric (non-equivalent) form of the equations is another difficulty. In fact, the first equation contains only the unknown *X* within a definite integral, while both unknown functions *X* and E_c are presented in the second equation. Let us mention again that the inequality of these equations also manifests itself in the presence of a scattered field in only one of them. Namely, the scattered field is the data source (sometimes exclusively) used to find the solution. Hence, for the solution, several general recommendations should considered: Eq. (5) is the final point of the calculation, since it contains the initial data and any model and/or assumptions using in the numerical procedure will eventually emerge here. Since the unknown *X* is within a definite integral, it is usually the case that any function up to constant is a solution of Eq. (5). Automatically, this will lead to solutions of E_c, and *p*, respectively. However, we cannot be sure that this is a real solution. Therefore, the form of the function *X* must be adequately chosen, and this can be done correctly using Eq. (6). Then, Eq. (5) is used to refine the parameters of the function *X* by minimizing the residuals.

According to Graf's theorem, the Hankel function can be expanded [20] to a sum of functions based on separate arguments:

$$H_0^{(2)}(k\,|\,\vec{r}-\vec{r}'|)=\sum_{n=-\infty}^{\infty}\begin{Bmatrix}J_n(k\rho)H_n^{(2)}(k\rho')\\J_n(k\rho')H_n^{(2)}(k\rho)\end{Bmatrix}\exp(in(\varphi-\varphi')),\quad\begin{matrix}\rho<\rho'\\\rho'<\rho\end{matrix} \tag{8}$$

Substituting (8) into (2) and multiplying both sides of (2) by *exp(im$_\varphi$)* and integrating across the angle φ, we obtain the scattered field at a distance *R* from the centre of the cylinder:

$$\int_0^{r_c}d\rho\int_0^{2\pi}d\varphi\,J_m(k\rho)X\exp(-im\varphi)=1/(2\pi H_m^{(2)}(kR))\int_0^{2\pi}d\varphi(E_z^{inc}(R,\varphi)-E_z(R,\varphi))\exp(-im\varphi) \tag{9}$$

After the summation of Eq. (9) in all *m*, we have

$$\int_0^{r_c}d\rho\int_0^{2\pi}d\varphi\,X\exp(-ik\rho\sin(\varphi))=1/(2\pi)\sum_{m=-\infty}^{\infty}\int_0^{2\pi}d\varphi(E_z^{inc}-E_z)\exp(-im\varphi)/H_m^{(2)}(kR) \tag{10}$$

Despite the infinite interval of the summation, we can neglect contribution to the sum of terms with $|m| > 20$.

Thus, on the left-hand side of (10), there exists only information about the fields inside the object, while the right-hand side is completely determined by the scattered field data. The equality of (10) can be used as a criterion for the adequacy of the model, as well as a basis for the development of different iterative schemes for inhomogeneous cases.

3. OPTIMIZED DATA CALCULATION FOR SOLVING THE INVERSE SCATTERING PROBLEM

Far-field measurements are the main initial data for the inverse electromagnetic scattering problem and are used to extract information about the object: size, shape, material parameters, etc. Eq. (10) can be used to calculate the dielectric constant for the known cylinder size, incident waveform and scattered field data. However, for practical purposes, we will make use of Eq. (9) as well. The fact is that the additional integration over the angle, leading from Eq.(9) to Eq.(10), smoothes the difference between the modeled and measured values, while that difference is an important criterion for choosing the optimal value. Therefore, to find the optimal parameters, we use Eq. (9). Since Eq. (9) is accurate, then it is approximately satisfied if the measured value is used instead of *Ez(R,φ)*.

Afterwards, to find the optimal parameters, we must require the minimum of the sum of the deviations for all values of *m*. As a result, the function to be minimized is shown as follows:

$$F(\varepsilon,r_c)=\sum_{m=-\infty}^{\infty}(L_m-P_m)^2 \tag{11}$$

where L_m and P_m are on the left and right sides of Eq. (9), respectively. Here, the dependence of the function F on the dielectric constant ε and the radius of the cylinder r_c as on the parameters are highlighted.

A schematic representation of the considered scattering process is shown in Fig. 1. A plane wave irradiates a dielectric cylinder. The incident direction is chosen to be the *x*-axis. The scattered field is fixed along a circle of radius *R* around the cylinder. All distances in the present work are measured in units of wavelength.

One of the important calculation parameters is the choice of the number of points *N* for which the internal field E_c is to be calculated (see (3-4)). Generally, the described procedure applies to any *N*, but it is obvious that for a sufficiently small *N,* the final result will lead to an insufficient value of ε. It is easily seen that as the radius increases, the minimum acceptable number of points also increases, which consequently leads to an increase in computation time. Here, we use r_c=1.3÷2.3, and $\Delta x=0.04$ as the distance between points.

The computational procedure is as follows. First, we calculate the internal field E_c according to Eq.(3,6). Then, for given values of ε_c and r_c, we calculate the scattered field E_L. This field is the exact solution to the forward problem and is considered as the "measured" field. To simulate the solution of the inverse problem, we need to calculate the function F for the set of test values of the cylinder radius r_c (or dielectric constant ε_c) assuming a given ε_c (or r_c). Having calculated values of the scattered field for a number of dielectric constant (cylindrical radius) values, we then compare them with the actual measured values. To minimize random measurement errors, we actually calculate the standard deviation according to Eq. (11). As a result, the problem of determining ε_n is reduced so as to find the minimum value of F among those computed for the given values of ε_j. Comparing these values, we select the optimal value of dielectric constant ε.

To examine the outlined procedure, we calculated F for different values of the refractive index n for the cylindrical radius r_c =2. These dependencies depicted on Fig. 2 demonstrate the possibility of identifying ε by comparing the modeled and measured field values. We also calculated F for different values of the cylindrical radius for dielectric constant ε=*1.5* (Fig. 3). In this case, the chances of identifying the radius at a fixed ε turn out to be higher: the additional minima, as can be seen, are quite far from being zero. That is, the comparison with the actual measured curve will lead to the optimal choice due to the use of the principle of minimum deviation according to (9).

If there is not enough scattered field data, then the final result will certainly be wrong. Of course, more measurements can be taken, or more points can be simulated. However, the problem is to determine the minimum number of points required for a reliable solution to the inverse problem. Fig. 4 partially illustrates this problem. If we perform the calculation with only 20 points, then the function F will be far from vanishing. Moreover, F = 0 is realized only by increasing n. It should also be noted that the position of the minimum value of the function F remains unchanged. However, for practical cases, it will be necessary to consider measurement errors for other analyses.

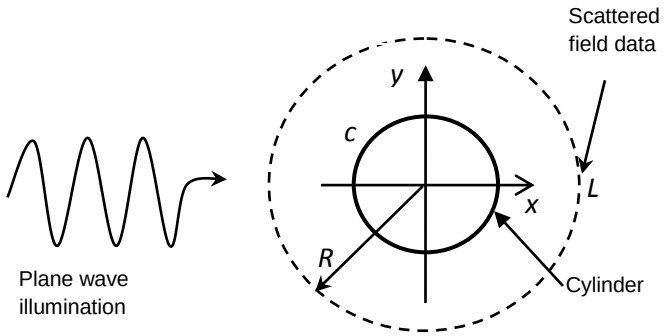

Fig. 1. Top view of the dielectric cylinder illuminated by a plane wave

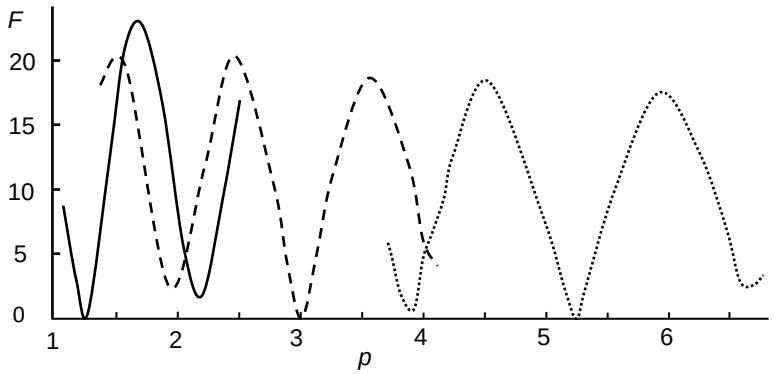

Fig. 2. Difference between modeled (n=n_c) and simulated (for different n) scattered field amplitudes. (p=n^2-*1*). r=2.0; n: 1.5 - solid; 2.0 - dashed; 2.5 – dotted

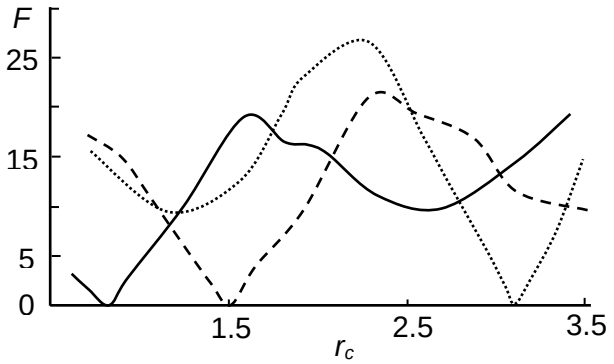

Fig. 3. Difference between modeled (for $r=r_c$) and simulated (for different r) scattered field amplitudes. ε=1.5; r_c: 1.2 - solid; 1.5 - dashed; 2.3 – dotted

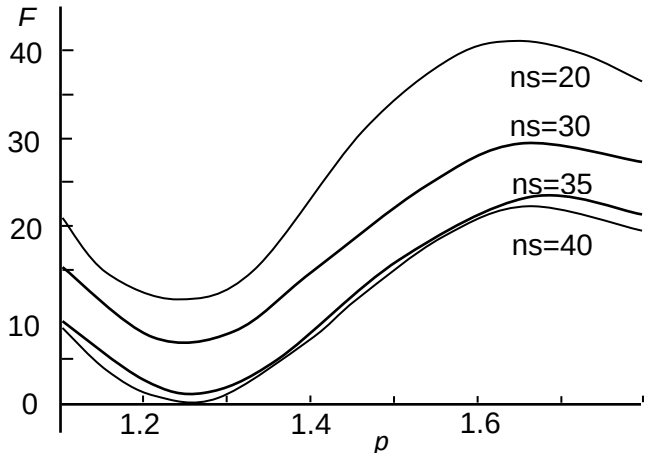

Fig. 4. Difference between modeled and simulated scattered field amplitudes for different number of the measured data ns. n=1.5; r=2.0

4. CONCLUSION

The forward scattering problem is to compute the scattered field for a given scatterer size and material parameters. Correspondingly, the inverse scattering problem recovers the input data from the scattered field data. The material parameters, scatterer size, and initial data of the field can be considered as input data. In this paper, the possibility of recovering the dielectric constant and/or cylindrical radius from the scattered field data set has been considered. Using the equation that confines the near-field and far-field amplitudes, we have calculated the differences between the modeled and measured fields for a definite number of points. By requiring a summation minimum for all these deviations, we determined the optimal parameters for the sample. The procedure has been demonstrated for dielectric cylinders. Potentially, the proposed method is also suitable for determining the sizes of other objects.

COMPETING INTERESTS

Authors have declared that no competing interests exist.

REFERENCES

1. Colton D, Kress R. Inverse acoustic and electromagnetic scattering theory. New York: Springer; 1998.
2. Borden B. Mathematical problems in radar inverse scattering. Inverse Problems. 2001;18(1):1-28.
3. Greene C, Wiebe P, Burczynski J, et al. Acoustical detection of high-density krill demersal layers in the submarine canyons off georges bank. Science. 1988; 241(4863):359-361.
4. Verschuur D, Berkhout A. Estimation of multiple scattering by iterative inversion,

part ii: Practical aspects and examples. Geophysics. 1997;62(5):1596-1611.
5. Henriksson T, Joachimowicz N, Conessa C, et al. Quantitative microwave imaging for breast cancer detection using a planar 2.45 GHz system. IEEE Trans. Instrum. Meas. 2010;59(10):2691-2699.
6. Kagiwada H, Kalaba R, Timko S, et al. Associate memories for system identification: Inverse problems in remote sensing. Mathem. Comp. Modelling. 1990; 14:200–202.
7. Quarteroni A, Formaggia L, Veneziani A. Complex systems in biomedicine. New York: Springer; 2006.
8. Wang Y, Chew W. An iterative solution of the two-dimensional electromagnetic inverse scattering problem. Int. J. Imag. Syst. Techn. 1989;1:100-108.
9. Vogeler M. Reconstruction of the three-dimensional refractive index in electromagnetic scattering by using a propagation–backpropagation method. Inverse Problems. 2003;19:739-753.
10. Geffrin JM, Chaumet P, Eyraud C, et al. Electromagnetic three-dimensional reconstruction of targets from free space experimental data. Appl. Phys. Lett. 2008; 92:194103(1-4).
11. Kirsch A, Ritter S. A linear sampling method for inverse scattering from an open arc. Inverse Probl. 2000;16(1):89–105.
12. Agarwal K, Chen X, Zhong Y. A multipole-expansion based linear sampling method for solving inverse scattering problems. Opt. Expr. 2010;18(6):6366-6381.
13. Hagemann F, Arens T, Betcke T, et al. Solving inverse electromagnetic scattering problems via domain derivatives. Inverse Probl. 2019;35:084005.
14. Haddar H. The interior transmission problem for anisotropic Maxwell's equations and its applications to the inverse problem. Math. Meth. Appl. Sci. 2004;27:2111–2129.
15. Thanh N, Beilina L, Klibanov M, et al. Reconstruction of the refractive index from experimental backscattering data using a globally convergent inverse method. SIAM J. Sci. Comput. 2014;36(3):B273–B293.
16. Taflove A, Hagness S. Computational electrodynamics: The finite-difference time-domain method. Boston: Artech House; 2005.
17. Chen Z, Taflove A, Backman V. Photonic nanojet enhancement of backscattering of light by nanoparticles: A potential novel visible-light ultramicroscopy technique. Opt. Express. 2004;12:1214-1220.
18. Abramov A, Kostikov A, Yue Y. Scattering of electromagnetic wave by system of core / shell microsphere and nanoparticle. J. Adv. Electromagn. 2020;1(9):32-34.
19. Richmond J. Scattering by a dielectric cylinder of arbitrary cross section shape. IEEE trans. Ant. Prop. 1965;13(3):334-341.
20. Abramovits J, Stigan I. Handbook on special functions. Moscow: Nauka; 1979.

Peer-review history:
The peer review history for this paper can be accessed here:
http://www.sdiarticle4.com/review-history/69367